HOSTED BY

ELSEVIER

Available online at www.sciencedirect.com

ScienceDirect

Soils and Foundations 60 (2020) 413–424

www.elsevier.com/locate/sandf

Technical Paper

Breakout force required for jack-up spudcan extraction from sand-over-clay seabeds

Pan Hu [a,*], Mark Cassidy [b], Fauzan Sahdi [c,d,1], Sam Stanier [e]

[a] School of Engineering, Western Sydney University, Kingswood, NSW 2747, Australia
[b] Melbourne School of Engineering, The University of Melbourne, Parkville, VIC 3010, Australia
[c] Centre for Offshore Foundation Systems, University of Western Australia, 35 Stirling Highway, Crawley, WA 6009, Australia
[d] Department of Civil Engineering, Universiti Malaysia, Sarawak, Malaysia
[e] Geotechnical and Environmental Research Group, University of Cambridge, Trumpington Street, Cambridge, Cambridgeshire CB2 1PZ, United Kingdom

Received 9 February 2019; received in revised form 31 December 2019; accepted 5 March 2020
Available online 21 April 2020

Abstract

Spudcan retrieval from clay soils remains a major concern offshore as the extraction force required to overcome suction and soil resistance often exceeds the pulling capacity available on the mobile jack-up, causing extensive delays. Although methods to calculate extraction resistance have been recently suggested for seabeds of pure clay, to date there is no guidance available for the commonly encountered sand-over-clays. Based on failure mechanisms observed in half-spudcan visualisation tests, and calibrated against an extensive geotechnical centrifuge database of precisely measured extractions, this paper presents a method for calculating the force required to extract the spudcan foundations of mobile jack-up platforms after they have penetrated through a sand layer into underlying clay. Complexities, such as the strength degradation and strength recovery of the underlying clay soil, that occurs during spudcan installation and jack-up operations, are accounted for. Validation of the proposed method is demonstrated by retrospective prediction of the centrifuge testing database. The method outlined will allow operators of jack-up platforms to assess the extraction force prior to jack-up installation and to plan operational scenarios based on seabed conditions.

Keywords: Centrifuge modelling; Clays; Sands; Consolidation; Spudcan foundation

1. Introduction

Self-elevated mobile jack-up units play an important role in offshore drilling in shallow waters, up to approximately 150 m depth. A jack-up hull is roughly triangular in shape and has three retractable truss-work legs. Jack-ups stand on inverted conical "spudcan" footings that can be in excess of 20 m in diameter (D) and can be penetrated in a wide range of soil conditions. During installation the legs are lowered to the seabed and self-weight of the jack-up places vertical loads on the spudcans. A preloading process, where water is pumped into ballast tanks in the jack-up hull, subjects the spudcans to further vertical load, and ensures that the footings have sufficient bearing capacity to withstand the jack-up's self-weight and potential environmental storm loads during operations. In seabeds of sand-over-clay this installation and preloading can push the spudcans through the sand layer into the underlying clay (Randolph et al., 2005; Dean, 2010).

Peer review under responsibility of The Japanese Geotechnical Society.
* Corresponding author.
E-mail addresses: p.hu@westernsydney.edu.au (P. Hu), mark.cassidy@unimelb.edu.au (M. Cassidy), fauzan.sahdi@uwa.edu.au (F. Sahdi), sas229@cam.ac.uk (S. Stanier).
[1] On postdoctoral leave.

https://doi.org/10.1016/j.sandf.2020.03.004
0038-0806/

Nomenclature

c_r	'operational' coefficient of consolidation
d	spudcan penetration depth from the soil surface
d_e	distance from the far edge of the spudcan influence zone to the edge of the sand column
D	diameter of the spudcan
e_0	void ratio of clay
F(n)	drain spacing factor
h_{br}	breakout depth
h_c	spudcan depth in the underlying clay layer
h_f	length of the shear surface in the sand layer
h_{final}	final penetration depth of spudcan
h_t	height of the spudcan top shoulder
H_s	sand thickness
I_D	relative density of sand
k	shear strength gradient
k_0	coefficient of earth pressure at rest
k_r	radial permeability at the initial specific volume
m	plastic volumetric strain ratio
n	drain spacing ratio
n_c	cycle number
N	NCL specific volume at $\sigma'_v = 1$ kPa
N_{95}	rate of strength degradation
OCR	over-consolidation ratio
q_{br}	ultimate breakout resistance
q_{in}	ultimate installation resistance
$q_{br\text{-}0}$	breakout resistance with no time for consolidation
$q_{br,\ predicted}$	predicted ultimate breakout resistance
$q_{br,\ test}$	measured ultimate breakout resistance
Q_{in}	ultimate installation force
Q_{br}	breakout force
$Q_{shear,\ clay}$	shear resistance of the clay mobilised along the vertical planes of the soil column
$Q_{shear,\ sand}$	shear resistance in the sand mobilised along the vertical plane of the soil column
r_e	radius of soil cylinder
r_w	radius of the sand column above the spudcan
R	a parameter that controls the position of the failure stress between the CSL and RSL
S_t	soil sensitivity
s_u	shear strength of clay
$s_{u,\ initial}$	initial undrained shear strength
s_{um}	shear strength of clay at sand-clay interface
t	diameter of the spudcan shaft
t_r	consolidation time
T_r	time factor
u	excess pore pressure
u_{max}	maximum excess pore pressure
U	degree of consolidation
v	specific volume
W_{sand}	weight of the sand column above the spudcan
z	depth from the original clay surface
γ'_c	submerged unit weight of clay
γ'_s	submerged unit weight of sand
γ_w	unit weight of water
κ	slope of the unload-reload line
λ	slope of the NCL (and CSL) line
Γ	specific volume at $\sigma'_v = 1$ kPa on the CSL line
μ	strength parameter
ϕ_{cv}	critical state friction angle of sand
ϕ'	mean triaxial compression friction angle
σ'_r	in situ radial effective stress
σ'_v	vertical effective stress
$\sigma'_{vE\text{-}n}$	vertical effective stress on the CSL at the current n_c

On completion of jack-up operations at a site, the legs are retracted from the seabed by lowering the hull into the water, thereby generating a buoyant uplift force and inducing tensile forces in the leg trusses. Successful leg extraction within a short period of time is preferred as this will allow for efficient redeployment of the rigs in other locations. However, in some instances the extraction may be difficult and time consuming because the pull-out capacity of the rig is less than the extraction resistance of the spudcans. Spudcan extraction from deep penetrations into clay (that can be in excess of two spudcan diameters) can take several days, and sometime longer (McClelland et al., 1981). Adding to lost productivity associated with the delay, prolonged hull submersion under the action of wave and current also poses risks of structural damage to the jack-up.

The industry standard guidelines for jack-up operations ISO (2012) note that potential leg extraction difficulties should be addressed prior to placement of the jack-up on site. However, only a few analytical methods for predicting the extraction resistance are available and these are limited to purely clay soils (Purwana et al., 2005; Purwana, 2007; Kohan et al., 2014a,b; Kohan, 2015). Hossain et al. (2015) demonstrated through geotechnical centrifuge experiments that a spudcan penetrating through a thin layer of surface sand eases the extraction force required, even for spudcans buried deep in the underlying clay. However, a practical and verified method to estimate the ultimate spudcan extraction resistance in sand-over-clay is currently unavailable in either the industry recommended practices or literature in the public domain. This paper presents such a method. A simple calculation procedure for predicting ultimate extraction resistance of spudcans in sand-over-clay soils is established. It accounts for both the degradation of clay strength during spudcan installation and the recovery of strength due to reconsolidation

of the clay layer under self-weight during jack-up operations.

2. Background

Purwana et al. (2005) experimentally investigated the influence of base suction on extraction of jack-up spudcans from single layer clay. It is found that the base suction is the main contributor for the larger breakout force required to extract spudcans with longer operation periods.

The installation, operation and subsequent extraction of the spudcan foundation of a jack-up drilling rig requires the effects of remoulding and reconsolidation to be assessed (e.g. Stewart and Finnie, 2001; Gan et al., 2012). Significant changes in strength can occur owing to consolidation as the excess pore water pressures generated from the spudcan penetration gradually dissipate and the soil strength recovers. To assess these changes in soil strength, it is necessary to adopt a framework that captures both the loss of strength from remoulding as well as the gain in strength on account of reconsolidation. Based on centrifuge tests of spudcan extraction in normally consolidated soil, Kohan et al. (2014b) provided a prediction method to estimate the peak extraction resistance by considering the factors characterising the change in soil shear strength around the spudcan and the effect of the operation load and strength ratio. Bienen et al. (2015) have considered the effect of consolidation around a footing penetrating into the carbonate silty clay and proposed a simple framework to predict the effect of consolidation on the load-penetration curve of the footing. However, for sand-over-clay soil stratigraphy there is no established design methodology for assessing the strength recovery after the operation and the resulting change in extraction force of a spudcan foundation.

There has now been a significant number of geotechnical centrifuges tests of spudcans penetrating sand-over-clay soils (e.g. Craig and Chua, 1990; Teh et al., 2010; Lee et al., 2013; Hu et al., 2014; Hu and Cassidy, 2017). Although some extraction results are shown in the resulting publications, all of these tests have concentrated on developing new understanding and numerical prediction of the installation punch-through events. Lee (2009) and Hu et al. (2014) carried out spudcan penetration-extraction tests on two-layer dense silica sand ($I_D = 92\%$) and medium dense silica sand ($I_D = 43\%$) over soft kaolin clay deposits. Details of the engineering properties of the University of Western Australia (UWA) kaolin clay and UWA super fine silica sand can be found in Lee et al. (2013). Safinus (2016) also investigated the spudcan penetration-extraction behaviour in carbonate sand over kaolin clay, allowing the underlying clay to consolidate before measuring the extraction resistance. For silica sand over stiff kaolin clay, Hu and Cassidy (2017) conducted centrifuge model tests, investigating the punch-through failure potential. The operation period and its effect on the extraction force was also modelled but not reported. These tests form a comprehensive database to study extraction after penetrating a sand layer into an underlying clay.

Adding to the model spudcan experimental database, post-test bisection and half-spudcan visualisation experiments have also revealed that rather than being uplifted with the extracting spudcan, the sand plug trapped underneath the spudcan stayed at the installation depth (Craig and Chua, 1990; Hu et al., 2016). Also, a gap was found to form at the upper interface of the trapped sand layer. This indicates the spudcan was separated from the sand plug immediately upon extraction, which would allow for the release of suction at the spudcan base.

The present work emanates from the above study on spudcan extraction from sand-over-clay deposits and proposes a simple framework to predict the variation of undrained shear strength of the clay layer due to both strength degradation (during installation) and reconsolidation (during operation) effects. It allows the recovery of soil strength to be incorporated into the framework by including the dissipation of excess pore pressure during periods of operation. The framework validity is demonstrated by estimating the spudcan breakout force after the operation period in the underlying clay of the sand-over-clay soil.

3. Centrifuge tests and extraction resistance

Sample preparation was similar for all of the sand-over-clay centrifuge tests from which data are utilised in this manuscript (Lee et al., 2013; Hu et al., 2014; Safinus, 2016; and Hu and Cassidy, 2017). All these full-spudcan tests were conducted at a centrifuge acceleration of 200 g. Details of the soil properties and testing measurements are listed in Table 1. The clay slurry was initially normally consolidated at an acceleration of 300 g in the centrifuge. Then a fabric membrane was placed on top of the clay and sand was pluviated as a surcharge for further consolidation of the clay at 300 g. The sand and fabric membrane were then removed and a new layer of sand was laid again following the same procedure but without the fabric membrane. The target sand thickness was achieved by scraping the sand surface using a sheet aluminium scraping plate. All the spudcan penetration and extraction tests were conducted at 200 g, hence the soil was lightly over-consolidated. In this paper all of the centrifuge test details are described in terms of model dimensions while all the test results are presented in prototype dimensions.

The testing procedure for a typical full spudcan model test L1SP1 in Hu et al. (2014) (see Table 1) is illustrated in Fig. 1 and it includes the following three stages: (a) Installation: the spudcan was penetrated in flight at a displacement-controlled model rate of 0.254 mm/s. The penetration rate was determined such that drained behaviour in sand and undrained behaviour in clay were attained; (b) Operation: at the end of the installation stage, the spudcan was maintained under load control at the ultimate installation force for a period of time. For example, under 200 g centrifuge acceleration, 20 min model time is

Table 1
Summary of full-spudcan centrifuge tests

Reference	No.	Test name	Geometry				Sand		Clay			Prototype operational periods (month)	Results	
			Conical angle	H_s (m)	D(m)	H_s/D	I_D	γ'_s (kN/m^3)	s_{um} (kPa)	k (kPa/m)	γ'_c (kN/m^3)		q_{in}(kPa)	q_{br} (kPa)
Lee (2009) and Lee et al. (2013)	1	D1F30a	0°	6.2	6	1.03	0.92	10.99	17.7	2.1	7.50	0.015	1902.7	595.2
	2	D1F40a	0°	6.2	8	0.78	0.92	10.99	17.7	2.1	7.50	0.015	1467.8	412.0
	3	D1F50a	0°	6.2	10	0.62	0.92	10.99	17.7	2.1	7.50	0.015	918.7	394.0
	4	D1F60a	0°	6.2	12	0.52	0.92	10.99	17.7	2.1	7.50	0.015	804.8	224.0
	5	D1F70a	0°	6.2	14	0.44	0.92	10.99	17.7	2.1	7.50	0.015	725.2	264.9
	6	D1F80a	0°	6.2	16	0.39	0.92	10.99	17.7	2.1	7.50	0.015	855.3	285.0
	7	D1F40b	0°	4.1	8	0.51	0.92	10.99	16.3	2.1	7.50	0.015	980.2	313.3
	8	D1F50b	0°	4.1	10	0.41	0.92	10.99	16.3	2.1	7.50	0.015	915.9	380.1
	9	D1F60b	0°	4.1	12	0.34	0.92	10.99	16.3	2.1	7.50	0.015	864.3	268.6
	10	D2F30a	0°	6.7	6	1.12	0.92	10.99	19.1	2.1	7.50	0.015	1342.7	564.0
	11	D2F40a	0°	6.7	8	0.84	0.92	10.99	19.1	2.1	7.50	0.015	1376.0	432.1
	12	D2F60a	0°	6.7	12	0.56	0.92	10.99	19.1	2.1	7.50	0.015	1047.1	290.0
	13	D2F80a	0°	6.7	16	0.42	0.92	10.99	19.1	2.1	7.50	0.015	842.0	283.8
	14	D2F30b	0°	5.8	6	0.97	0.92	10.99	18.6	2.1	7.50	0.015	1902.5	497.4
	15	D2F40b	0°	5.8	8	0.73	0.92	10.99	18.6	2.1	7.50	0.015	1276.8	521.2
	16	D2F60b	0°	5.8	12	0.48	0.92	10.99	18.6	2.1	7.50	0.015	1100.5	368.0
	17	D2F80b	0°	5.8	16	0.36	0.92	10.99	18.6	2.1	7.50	0.015	849.2	283.1
	18	D2F30c	0°	4.8	6	0.80	0.92	10.99	17.9	2.1	7.50	0.015	1672.4	519.1
	19	D2F40c	0°	4.8	8	0.60	0.92	10.99	17.9	2.1	7.50	0.015	1486.0	602.2
	20	D2F60c	0°	4.8	12	0.40	0.92	10.99	17.9	2.1	7.50	0.015	1201.8	430.0
	21	D2F80c	0°	4.8	16	0.30	0.92	10.99	17.9	2.1	7.50	0.015	1037.0	371.0
	22	D2F30d	0°	3.4	6	0.57	0.92	10.99	16.6	2.1	7.50	0.015	1278.7	512.2
	23	D2F40d	0°	3.4	8	0.43	0.92	10.99	16.6	2.1	7.50	0.015	1110.2	428.4
	24	D2F60d	0°	3.4	12	0.28	0.92	10.99	16.6	2.1	7.50	0.015	965.2	362.0
	25	D2F80d	0°	3.4	16	0.21	0.92	10.99	16.6	2.1	7.50	0.015	983.7	333.1
	26	D1SP40a	13°	6.2	8	0.78	0.92	10.99	17.7	2.1	7.50	0.015	1263.5	414.5
	27	D1SP50a	13°	6.2	10	0.62	0.92	10.99	17.7	2.1	7.50	0.015	1283.1	315.6
	28	D1SP60a	13°	6.2	12	0.52	0.92	10.99	17.7	2.1	7.50	0.015	971.9	298.4
	29	D1SP70a	13°	6.2	14	0.44	0.92	10.99	17.7	2.1	7.50	0.015	859.1	227.5
	30	D1SP80a	13°	6.2	16	0.39	0.92	10.99	17.7	2.1	7.50	0.015	747.6	228.0
Hu et al. (2014)	31	L1SP1	13°	6.0	6	1.00	0.43	9.96	13.0	1.5	7.11	0.015	1747.3	601.0
	32	L1SP2	13°	6.0	8	0.75	0.43	9.96	13.0	1.5	7.11	0.015	812.1	268.3
	33	L1SP3	13°	6.0	10	0.60	0.43	9.96	13.0	1.5	7.11	0.015	842.9	188.4
	34	L1SP4	13°	6.0	12	0.50	0.43	9.96	13.0	1.5	7.11	0.015	1032.0	258.4
	35	L1SP5	13°	6.0	14	0.43	0.43	9.96	13.0	1.5	7.11	0.015	852.6	187.5
	36	L2SP1	13°	5.0	6	0.83	0.43	9.96	12.4	1.5	7.11	0.015	1209.5	461.0
	37	L2SP2	13°	5.0	10	0.50	0.43	9.96	12.4	1.5	7.11	0.015	768.7	229.3
	38	L2SP3	13°	5.0	14	0.36	0.43	9.96	12.4	1.5	7.11	0.015	569.0	160.3
	39	L2SP4	13°	5.0	16	0.31	0.43	9.96	12.4	1.5	7.11	0.015	491.6	150.5
	40	L2SP5	13°	5.0	20	0.25	0.43	9.96	12.4	1.5	7.11	0.015	382.8	135.2
	41	L3SP1	13°	3.2	6	0.53	0.43	9.96	11.0	1.6	7.11	0.015	865.6	333.9
	42	L3SP2	13°	3.2	8	0.40	0.43	9.96	11.0	1.6	7.11	0.015	680.6	267.9
	43	L3SP3	13°	3.2	12	0.27	0.43	9.96	11.0	1.6	7.11	0.015	594.6	206.6
	44	L3SP4	13°	3.2	16	0.20	0.43	9.96	11.0	1.6	7.11	0.015	427.4	138.1
	45	L3SP5	13°	3.2	20	0.16	0.43	9.96	11.0	1.6	7.11	0.015	339.4	114.5

Safinus (2016)	46	B1D12	15°	6.8	12	0.57	0.20	7.38	10.5	1.7	7.87	18.519	1245.0	392.0
	47	B1D15	15°	6.8	15	0.45	0.20	7.38	10.5	1.7	7.87	18.519	1101.0	372.0
Hu and Cassidy (2017)	48	SP1	13°	6.0	6	1.00	0.65	10.43	43.9	3.4	7.79	18.519	2059.0	834.3
	49	SP2	13°	6.0	8	0.75	0.65	10.43	43.9	3.4	7.79	18.519	1876.8	905.8
	50	SP3	13°	6.0	10	0.60	0.65	10.43	43.9	3.4	7.79	18.519	1666.7	483.8
	51	SP4	13°	4.0	8	0.50	0.65	10.43	32.6	3.5	7.79	18.519	1632.6	904.8
	52	SP5	13°	4.0	10	0.40	0.65	10.43	32.6	3.5	7.79	18.519	1747.3	707.1
	53	SP6	13°	4.0	12	0.33	0.65	10.43	32.6	3.5	7.79	18.519	1559.8	683.3

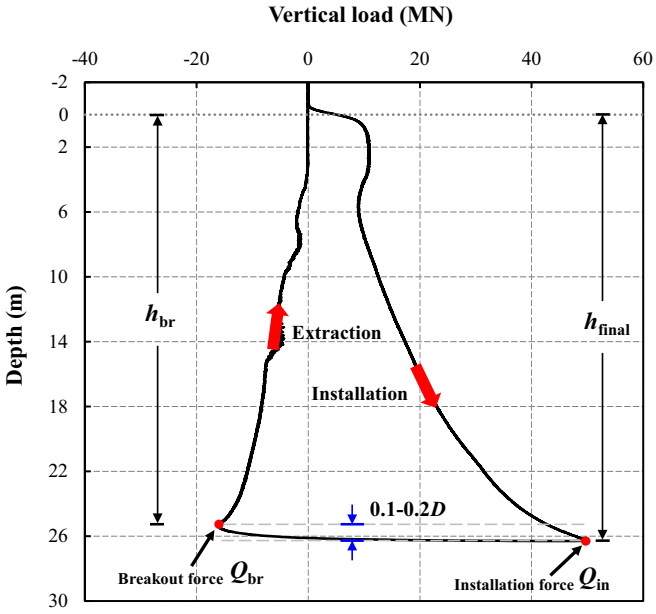

Fig. 1. A typical spudcan penetration and extraction resistance profile (L1SP1 in Hu et al., 2014).

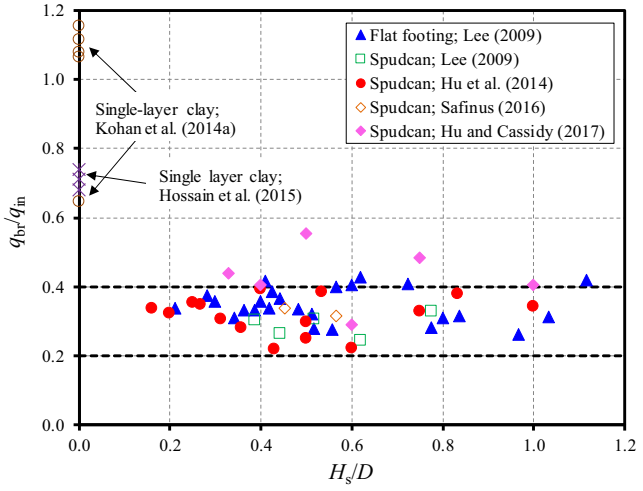

Fig. 2. The ratio of q_{br} and q_{in} from sand overlying clay testing database.

equivalent to approximately 1.52 years prototype operation period for a 30 mm diameter model spudcan. This models a jack-up unit under self-weight during its operational life; (c) Extraction: immediately after operation, the spudcan was pulled out with the same speed as that of penetration until the spudcan tip was clear of the soil surface.

The value of ultimate soil resistance force of a single leg to installation before the operation is referred to as Q_{in}. The net uplift force required to extract the leg from the soil has to exceed the soil resistance force to extraction, which is the so-called 'breakout force' Q_{br}. The breakout force Q_{br} is affected by several factors, including the physical characteristics of the soils, the depth of penetration, the

geometry of the spudcan and whether soil backfill has occurred. The corresponding equivalent stresses q_{in} and q_{br} ('Q' divided by the maximum cross-sectional area of the spudcan) and all other testing parameters from the centrifuge testing database are tabulated in Table 1. Fig. 1 also shows that for this particular test, the resistance during extraction is ~ 40% of that during penetration in sand-over-clay soil. The Q_{br} is normally developed after a spudcan has been raised over a very short displacement of about 0.1–0.2 spudcan diameter from its final penetration depth, referred to as h_{final}. The depth of mobilisation of the breakout force Q_{br} is referred to as the 'breakout depth', h_{br}. In the field and post-breakout, the leg extraction would be expected to be easier for the remaining extraction depth, at least for soil profiles with increasing strength with depth.

The ratio of extraction resistance to penetration resistance for tests with near-immediate extraction is in the range of 0.2–0.4, as shown in Fig. 2. Except test SP3, all the tests in Hu and Cassidy (2017) with a longer operating period have a higher ratio of q_{br}/q_{in} in the range of 0.4–0.6, indicating the clay strength has recovered to an extent resulting in higher pull-out force being needed to extract the spudcan foundations. This shows that the extraction force is much higher after allowing a period of operation and the effect of consolidation has to be considered when estimating the extraction force. For a single clay layer, the resistance during extraction in disturbed soil is 68%–74% of that during penetration in undisturbed soil (Hossain et al., 2015). However, the experimental results of Purwana et al. (2005) and Kohan et al. (2014a) indicate higher ratios due to longer operation periods. Compared with the extraction from a single clay layer, the reduction in the breakout force for sand-over-clay soil is clearly due to the immediate separation of the spudcan base from the trapped sand plug (i.e. a vented condition) and the immediate release of suction force.

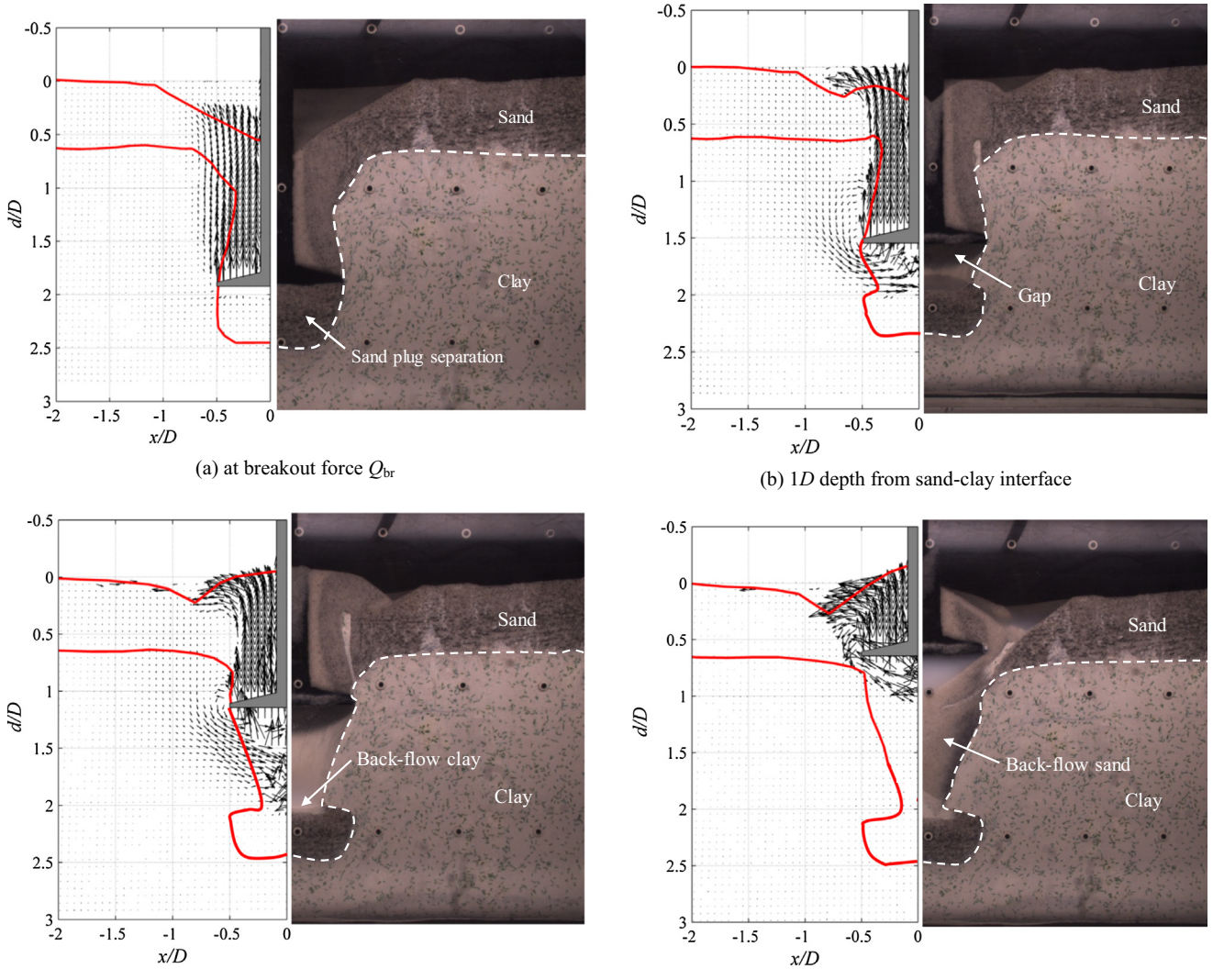

(a) at breakout force Q_{br}

(b) 1D depth from sand-clay interface

(c) 0.5D depth from sand-clay interface

(d) sand-clay interface

Fig. 3. Critical stages during spudcan extraction from sand-over-clay and development of soil deformations (H5C0 in Hu et al., 2016).

4. Extraction mechanisms

Half-spudcan geotechnical centrifuge tests were designed to penetrate and extract the spudcan adjacent to the strongbox window, permitting the soil deformation to be captured continuously in-flight by a digital machine vision camera sitting at right angles on a cradle within the channel (see Stanier and White, 2013 for further details on this system). One half-spudcan PIV test (only installation stage was originally reported in Hu et al., 2016) was used to investigate the extraction mechanism of a spudcan foundation in sand overlying clay soils. The aim was to reveal the soil failure mechanism, linking directly to the extraction resistance profile.

Fig. 3 depicts the soil flow mechanism at four critical stages of the extraction test H5C0 in Hu et al. (2016). The exposed plane of the model was seeded with coloured flock on the clay layer and black dyed sand on the sand layer. This seeding was done to improve the texture within the digital images and it was applied such that the artificial seeding ratio (ASR) was in the range of 0.4–0.6 (Stanier and White, 2013). The images captured by the camera were then analysed using Particle Image Velocimetry (PIV) (aka Digital Image Correlation or DIC) techniques (Stanier et al., 2015) incorporating photogrammetric corrections for camera lens and pose induced errors (White et al., 2003).

Fig. 3 illustrates the four key stages of the breakout mechanism: (a) at breakout force Q_{br}; (b) at a depth of $1D$ from the original sand-clay interface; (c) at a depth of $0.5D$ from the original sand-clay interface; and (d) at the original sand-clay interface. The solid lines in the LHS of the figure represent the sand surface and sand-clay interface, respectively.

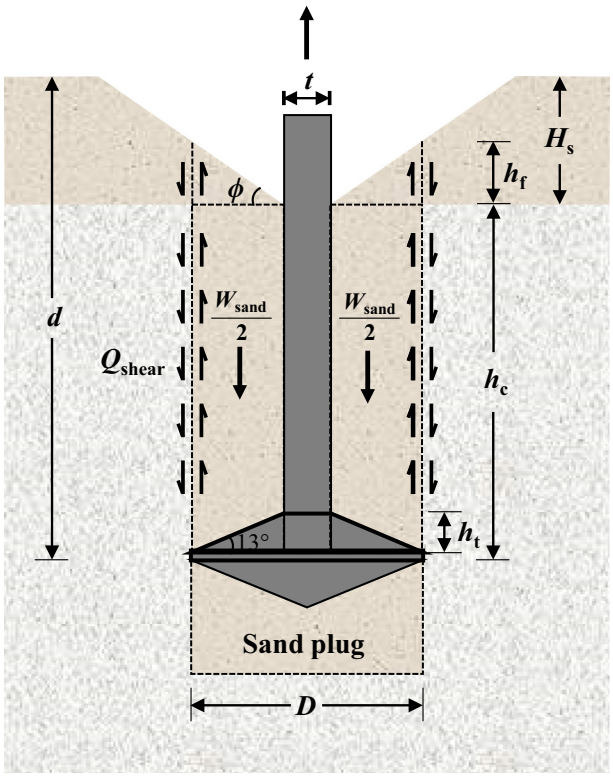

Fig. 4. Proposed mechanism during spudcan extraction from sand overlying clay.

At breakout force Q_{br}, shown in Fig. 3(a), it is clear that a column of soil is lifted above the spudcan, through both the sand and clay layers, and that suction is not mobilised at the base of the spudcan as immediate breakaway due to venting through the sand layer occurs. The shearing periphery of the column of soil being lifted is encompassed totally by the surrounding clay layer. It is the resistance of this soil and the weight of the column of soil within that will dictate the peak breakout resistance.

As the extraction progresses to a depth of $1D$ from the original sand-clay interface, shown in Fig. 3(b), clay begins to flow around the base of the column of sand being lifted, filling the void beneath the spudcan. The shearing periphery of the soil column being lifted also narrows and coincides with the vertical sand-clay interface generated by drag-down of sand during installation.

As extraction progresses to a depth of $0.5D$ from the original sand-clay interface, shown in Fig. 3(c), the clay backflow mechanism enlarges significantly whilst the shearing column of soil above the spudcan is totally encompassed by the sand layer. A cavity also begins to form immediately beneath the spudcan, into which sand flows as extraction progresses.

As the extraction nears completion at the depth of the original sand-clay interface, shown in Fig. 3(d), the sand surrounding the spudcan abruptly fails leading to rapid backfill of the cavity beneath the spudcan. This post-breakout stage also demonstrates that the underlying clay stopped moving and the soil movement was primarily above the spudcan and in the sand layer.

5. Proposed method

Based on the measurement from PIV analysis, the failure mechanism of soil above the spudcan is assumed to be a cylinder with an area equivalent to that of the spudcan maximum cross section area. The repose angle between the surface of the falling sand and the horizontal line immediately before the extraction is taken as equivalent to the critical state friction angle of sand (taken as 31° for the testing series in Table 1). This angle is used in the following model to correlate the relationship between the height of the shear surface in the sand and the spudcan diameter. A simplified method is proposed based on the breakout failure mechanism and the vertical uplift force equilibrium condition, as illustrated in Fig. 4. The failure mode is characterised by a column of sand being uplifted by the spudcan with an inverted cone of sand missing at the free surface as a result of sand flowing into the cavity generated by the spudcan during penetration. For simplification, a vertical sand-clay friction interface is assumed in the proposed model.

The spudcan extraction resistance is therefore comprised of three components: (a) weight of soil above the spudcan; (b) resistance along the shear plane generated above the spudcan in the clay layer; and (c) the same in the sand layer.

Based on the above analysis, the breakout force, Q_{br}, could be written as:

$$Q_{br} = W_{sand} + Q_{shear,\ clay} + Q_{shear,\ sand} \tag{1}$$

The weight of the sand column above the spudcan for the simplified geometry illustrated in Fig. 4, can be calculated as:

$$W_{sand} = \gamma'_s \left\{ \frac{\pi}{4} D^2 (h_c + h_f) - \frac{\pi t^2}{4} (h_c - h_t) - \frac{\pi (h_t + h_f)}{3} \left[\left(\frac{D}{2}\right)^2 + \left(\frac{D}{2}\right) \cdot \frac{t}{2} + \left(\frac{t}{2}\right)^2 \right] \right\} \tag{2}$$

where t is the diameter of the spudcan shaft; h_c is the spudcan depth in the underlying clay layer; h_f is the length of the shear surface in the sand layer; h_t is the height of the spudcan top shoulder; and γ'_s is the submerged unit weight of sand.

The shear resistance of the clay mobilised along the vertical planes of the soil column being uplifted is:

$$Q_{shear,\ clay} = \pi D h_c s_u \tag{3}$$

The s_u in Eq. (3) is taken as the average shear strength in the vicinity of the spudcan during the extraction process. Any change in clay shear strength associated with soil consolidation surrounding the spudcan occurring prior to or during extraction stage is a major influence factor, and this will be considered through a framework in the next section.

A simple lower bound for the shear resistance in the sand mobilised along the vertical plane of the soil column is:

$$Q_{shear,\ sand} = \pi D \tan\phi_{cv} \frac{\gamma'_s {h_f}^2}{2} \tag{4}$$

where ϕ_{cv} is the critical state friction angle of sand.

6. MODEL framework

As indicated in Eqs. (1) and (3), the prediction of the ultimate uplift capacity requires the determination of an operative shear strength that represents the average strength of the clay mobilised in shear around the periphery of the column of soil being uplifted above the spudcan, as illustrated in Fig. 3(a). The determination of the operative shear strength necessitates the consideration of the softening from the soil remoulding and strengthening from the consolidation. To this end, a framework based on critical state theory is proposed, where the changes in undrained shear strength during remoulding and consolidation are correlated to the changes in vertical effective stress level of the soil. The framework is presented in Fig. 5 and is based on the well-established relationship

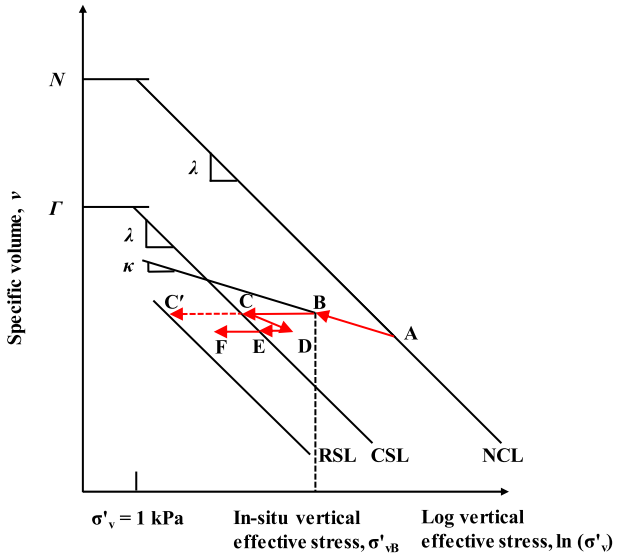

Fig. 5. Simplified critical state interpretation of remoulding and reconsolidation.

between the specific volume and the vertical effective stress, which has previously been used for modelling the behaviour of risers under episodic cyclic loading (White and Hodder, 2010; Hodder et al., 2013).

The underlying clay soil is initially normally consolidated at 300 g (point A in Fig. 5). It moves to point B after consolidation under the surcharge of sand. During spudcan penetration, the soil state moves to the critical-state line (CSL, point C in Fig. 5) at failure. This broadly corresponds to the shear strength values from the T-bar measurements for the initial penetration. As the vertical effective stress reduces from point B to point C at constant volume, excess pore pressure is generated. If the soil was fully remoulded, the soil state would move to point C′ on the remoulded strength line (RSL). The RSL represents the lowest stress state achievable at any given vertical effective stress σ'_v and the stress spacing ratio between the RSL and the CSL is taken as equal to the soil sensitivity, S_t.

During operation, the excess pore pressure dissipates causing the soil to reconsolidate, and the specific volume decreases (C to D) with a magnitude according to the slope of the unload-reload line (with slope κ) towards the initial stress. During extraction, the current stress of the soil initially moves to point E on the CSL line and moves further to point F. At this point, the clay shear strength corresponding to the extraction was mobilised.

Following the notation in White and Hodder (2010), the initial specific volume at point A (i.e. under normally consolidated conditions), v_A, can be determined as follows:

$$v_A = N - \lambda \ln(\sigma'_{vA}) \tag{5}$$

where N is the specific volume at $\sigma'_v = 1$ kPa and λ is the slope of the NCL (and CSL) line. After removal of the surcharge load, there is an increase in specific volume, Δ_v,

because the clay swells during unloading (point A to point B in Fig. 5). This change in specific volume is calculated as:

$$\Delta_v = \kappa \ln\left(\frac{\sigma'_{vA}}{\sigma'_{vB}}\right) \tag{6}$$

where the magnitude of Δ_v depends on the slope κ.

The specific volume at point B can thus be calculated as:

$$v_B = v_A + \Delta_v \tag{7}$$

During undrained penetration in the clay layer, $v_B = v_C$. Therefore, the vertical effective stress at point C can be calculated as:

$$\sigma'_{vC} = e^{\frac{\Gamma - v_C}{\lambda}} \tag{8}$$

where Γ is the specific volume at $\sigma'_v = 1$ kPa on the CSL line.

At any given σ'_v during shearing, the operative strength s_u can be calculated from the strength parameter, μ, as:

$$s_u = \mu \sigma'_v \tag{9}$$

The magnitude of μ is approximately 0.7 by matching the measured s_u with the corresponding σ'_v in the back-analysed tests as summarised in Table 1. Thus, the change in the undrained shear strength of the soil is proportional to the change in the vertical effective stress.

The initial undrained shear strength, $s_{u,\,initial}$ is expressed in terms of σ'_v and the over-consolidation ratio OCR (Wroth, 1984) as:

$$s_{u,\,initial} = \sigma'_v \left(\frac{s_u}{\sigma'_v}\right)_{NC} (OCR)^m \tag{10}$$

where $(s_u/\sigma'_v)_{NC}$ is the normally consolidated strength ratio and m is the plastic volumetric strain ratio. Optimal values of $(s_u/\sigma'_v)_{NC}$ and m were obtained by fitting Eq. (10) to the initial undrained shear strength profile recorded during the accompanying T-bar penetrometer experiment for each series of centrifuge tests as summarised in Table 1. Vertical penetration of the spudcan is assumed to generate an excess pore pressure field that dissipates one-dimensionally in the radial direction towards the sand plug (see Fig. 6).

The excess pore pressures generated by the installation process are assumed to dissipate during operation. The rate of dissipation in soil is governed by the coefficient of consolidation. In this one-dimensional radial consolidation approximation, we assume a single 'operational' coefficient of consolidation, c_r, (e.g. Muir Wood, 1990) to be representative of the radial consolidation characteristics of the column of soil above the spudcan:

$$c_r = \frac{k_r v_{0C} \sigma'_r}{\gamma_w \sqrt{\lambda \kappa}} \tag{11}$$

where v_{0C} is the specific volume for the in situ vertical effective stress at the end of the installation process σ'_{vC}; σ'_r is the in situ radial effective stress; γ_w is the unit weight of water and k_r is the radial permeability at the initial specific volume. As k_r is likely to dominate the rate of drainage

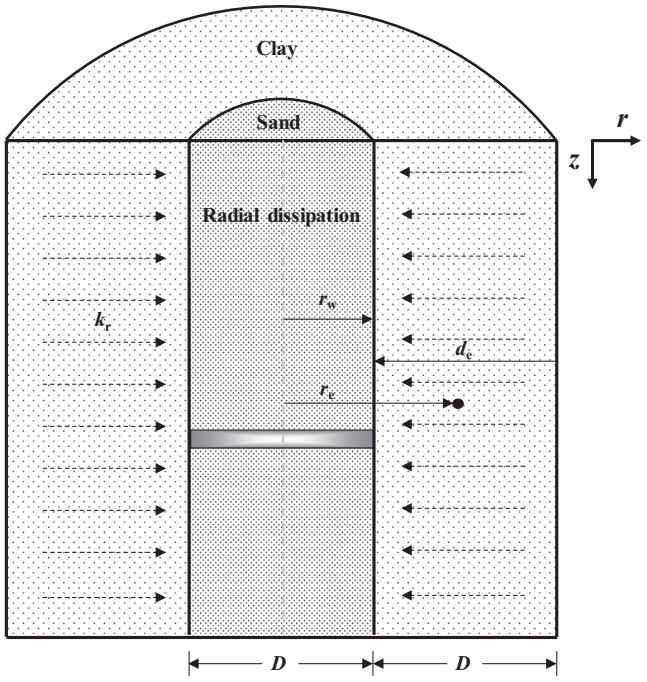

Fig. 6. Schematic of soil cylinder with vertical sand column drain.

around a spudcan, the following k_r expression of Al-Tabbaa and Wood (1987) is used in this analysis:

$$k_r = 1.49 e_0^{2.03} \times 10^{-9} \text{ m/s} \tag{12}$$

where e_0 is the void ratio of clay. It is shown in Houlsby and Hitchman (1988) that the drained resistance of a penetrometer varies directly with the in situ radial effective stress σ'_r. The expression proposed by Mayne and Kulhawy (1982) is employed in this paper:

$$\sigma'_r = k_0 \sigma'_v = (1 - \sin\phi')\sigma'_v OCR^{\sin\phi'} \tag{13}$$

where k_0 is the coefficient of earth pressure at rest. A mean triaxial compression friction angle ϕ' of 25° is recommended in Lehane et al. (2009) to provide a reasonable assessment of σ'_r values in the centrifuge tests. The degree of consolidation, U, in the underlying clay is given by (Barron, 1948):

$$U = 1 - \exp\left(\frac{-8T_r}{F(n)}\right) \tag{14}$$

where the time factor T_r is defined as

$$T_r = \frac{c_r t_r}{d_e^2} \tag{15}$$

where t_r is the consolidation time; and d_e is the distance from the far edge of the spudcan influence zone to the edge of the sand column. It has been shown in Teh et al. (2008) that soil flow induced by the spudcan penetration in sand-over-clay soil occurred within $1D$ from the spudcan edge, therefore the d_e is taken as $1D$ in this analysis. The F(n) is the drain spacing factor, given by

Table 2
Framework parameters for UWA kaolin clay.

Parameter	Symbol	Value	Reference
Normal consolidation line (NCL) or critical state line (CSL) slope	λ	0.26	Acosta-Martinez and Gourvenec (2006)
Unload-reload slope	κ	0.06	Stewart (1992)
CSL specific volume at $\sigma'_v = 1$ kPa	Γ	3.29	White and Hodder (2010)
Rate of strength degradation	N_{95}	2.5	Sahdi et al. (2017)
NCL specific volume at $\sigma'_v = 1$ kPa	N	3.67	White and Hodder (2010)

$$F(n) = \frac{n^2}{n^2-1}\ln(n) - \frac{3n^2-1}{4n^2} \tag{16}$$

where n is the drain spacing ratio, defined as

$$n = \frac{r_e}{r_w} \tag{17}$$

where r_e is the radius of soil cylinder, which is taken as the distance from the centre of the sand column to the centre of the spudcan influence zone (see Fig. 6). The corresponding penetration resistance represents the average response of many soil elements located at different offsets within the spudcan influence zone from the centreline of the spudcan path. The radius r_w is the radius of the sand column above the spudcan. Excess pore pressure, u, is generated in response to undrained shearing caused by the penetration of the spudcan. The maximum excess pore pressure, u_{max}, at a given specific volume is expressed as (illustrated in Fig. 5):

$$u_{max} = \sigma'_{vB} - \sigma'_{vC} \tag{18}$$

As shown in Fig. 5, during consolidation, the excess pore pressure may partially (or fully) dissipate causing an increase in vertical effective stress, where the vertical effective stress at point D is:

$$\sigma'_{vD} = \sigma'_{vC} + \Delta\sigma'_v = \sigma'_{vC} + u_{max}U \tag{19}$$

The difference between the post-penetration vertical effective stress σ'_{vC} and the reconsolidated vertical effective stress, σ'_{vD} indicates the change in vertical effective stress during reconsolidation. The pore pressure dissipation leads to a corresponding change in specific volume values, which can be expressed as:

$$\Delta v = -\kappa \ln\left(\frac{\sigma'_{vD}}{\sigma'_{vC}}\right) \tag{20}$$

Therefore, the specific volume at point D can be expressed as:

$$v_D = v_C + \Delta v \tag{21}$$

During extraction, the positive excess pore pressure results in a current vertical effective stress σ'_{vF}, which is a proportion of the stress at the critical state line corresponding to the current specific volume, v ($\sigma'_{vE\text{-}n}$)

$$\sigma'_{vF} = R\sigma'_{vE\text{-}n} \tag{22}$$

where $\sigma'_{vE\text{-}n}$ is the vertical effective stress on the CSL at the current cycle number n_c, and so is linked to the current specific volume by

$$\sigma'_{vE\text{-}n} = e^{\frac{\Gamma - v_D}{\lambda}} \tag{23}$$

The parameter R controls the position of the failure stress, σ'_{vF}, between the CSL and RSL and can be written as

$$R = \frac{1}{S_t} + \left(1 - \frac{1}{S_t}\right)e^{\frac{-3(n_c - 0.25)}{N_{95}}} \tag{24}$$

where N_{95} is the rate of strength degradation. The cycle number n_c is calculated following Randolph et al. (2007): the first penetration is designated as $n_c = 0.25$; for extraction in this analysis, the n_c is incremented by 0.5 (i.e. $n = 0.75$).

Finally, the shear strength corresponding to point F is calculated according to Eq. (9) by taking $\sigma'_v = \sigma'_{vF}$. The parameters within the framework, along with appropriate values, are detailed in Table 2.

7. Performance of the proposed method

A large number of centrifuge model tests investigating punch-through failure in sand-over-clay soil have been reported with full (i.e. including extraction) spudcan penetration-extraction profiles (Lee, 2009; Hu et al., 2014; Safinus, 2016; Hu and Cassidy, 2017). The measured extraction force for different operational periods is considered in the database, which is used to validate the newly proposed prediction method and assess its performance.

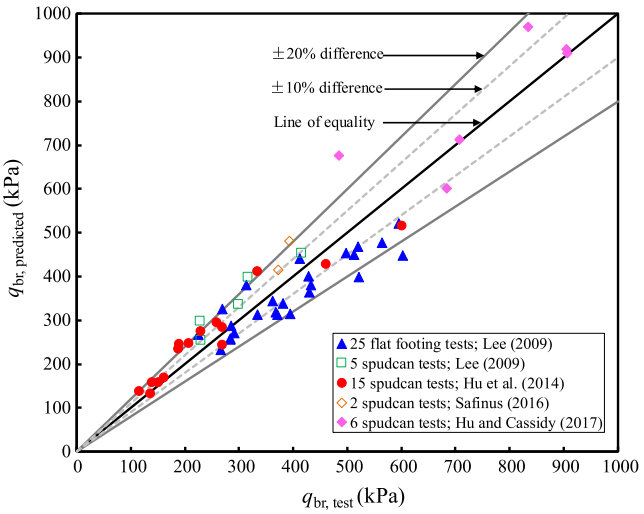

Fig. 7. Comparison of breaking force from centrifuge tests and the proposed predictive model.

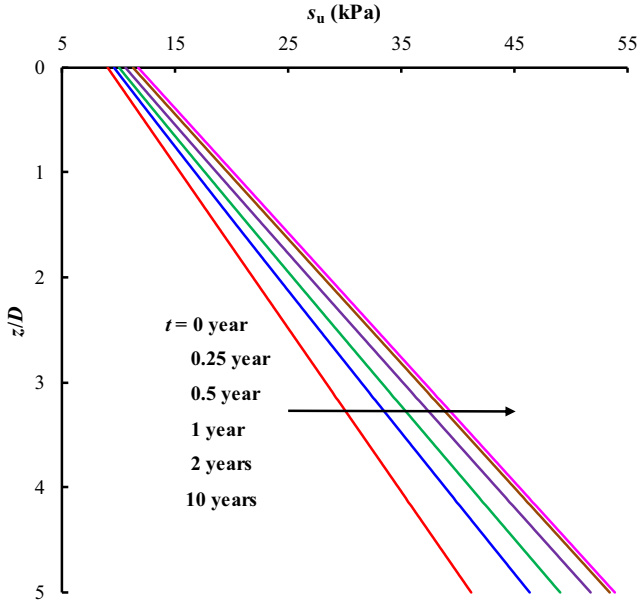

Fig. 8. Shear strength prediction of test L1SP1 according to different consolidation time (0 year, 0.5 year, 1 year, 2 years and 10 years).

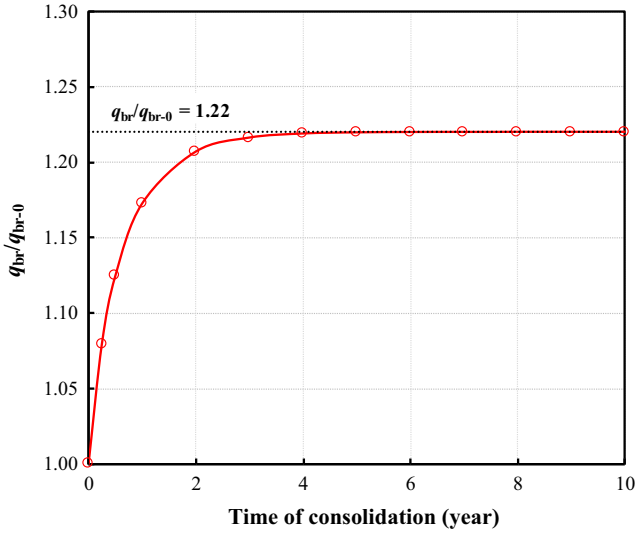

Fig. 9. Normalised extraction force of test L1SP1 for different consolidation time.

It should be noted that 53 centrifuge tests constitute the database, and that the database is limited to the silica and carbonate sands and kaolin clays. As shown in Fig. 7, 42 predicted data $q_{br,\ predicted}$ fall within ± 20% difference of the measured value $q_{br,\ test}$ and 20 predicted data has a difference of less than 10%. For the tests with prototype operation period of 1.52 years in Hu and Cassidy (2017), three predicted values show the difference of less than 1.4% to the measured values. The method generates reasonably good predictions for the tests with immediate extraction of the spudcan foundation and more importantly for those with significant operational periods.

For a typical test L1SP1 in Table 1, the undrained shear strength for consolidation time of 0 year to two years with increment of half year and two to ten years with increment of one year were calculated from the framework as shown in Fig. 8. The breakout resistance calculated for the corresponding consolidation time normalised by the breakout resistance with no time (0 year) for consolidation ($q_{br\text{-}0}$) are shown in Fig. 9. With consolidation, the clay soil regains strength, and the breakout resistance during immediate uplift increases rapidly in the first two years before converging to a value of around 1.22 times the nominal capacity in the duration of four to ten years. This shows that in some instances the initial clay strength can be exceeded as a consequence of reconsolidation, however, the likelihood of this is dependent upon the in-situ vertical effective stress profile and the sensitivity of the clay. This example also indicates that the effect of consolidation must be properly considered when estimating the breakout resistance of the spudcan foundation in sand-over-clay soil for anything but the shortest of operational periods.

As a crude first estimate, the Hu et al. (2014) method could be used to calculate the maximum penetration force Q_{in}, before multiplying Q_{in} by a factor in the range of 0.2–0.4 for immediate extraction or 0.4–0.6 for a period of reconsolidation (as indicated in Fig. 2) to estimate Q_{br}. This could then be followed by the more in-depth calculation proposed in this paper, which can also be used to generate breakout resistances for varying operational periods.

8. Conclusions

Centrifuge tests have been performed to investigate spudcan extraction resistance in UWA super fine silica sand overlying kaolin clay soil. The centrifuge tests on the extraction of half-spudcan with subsequent PIV analysis revealed that the breakout of the spudcan was mainly governed by a cylindrical shear failure mechanism directly above the spudcan.

A critical state framework was proposed to describe the variation of the operative soil strength with remoulding and reconsolidation. Consolidation effects are included in the framework by linking the excess pore pressure to a simple radial dissipation model, which is used to predict the reduction in specific volume caused by consolidation that in turn results in recovery of undrained shear strength. The simple prediction method together with the framework can capture the key aspects of the soil behaviour and predict the breakout force of a spudcan foundation in sand overlying clay soil for a wide range of degree of consolidation. This paper provides a study of the effect of consolidation on the breakout resistance of the spudcan foundation.

The present study has shown that a simplified method for predicting the breakout force at a site with sand-over-clay stratigraphy can be established. This helps the operators to plan appropriate operational measures based on such seabed conditions and operational periods.

Acknowledgement

This work forms part of the activities of the Centre for Offshore Foundation Systems (COFS) at the University of Western Australia, Australia, which is supported by the Lloyd's Register Foundation. Lloyd's Register Foundation invests in science, engineering, and technology for public benefit, worldwide. This project received additional support from the ARC Laureate Fellowship FL130100059 of the second author. The last author was supported by ARC DECRA Fellowship DE170100119.

References

Acosta-Martinez, H.E., Gourvenec, S.M., 2006. One-dimensional consolidation tests on kaolin clay. Research Report GEO: 06385, University of Western Australia, Geomechanics Group, Perth.

Al-Tabbaa, A., Wood, D.M., 1987. Some measurements of the permeability of kaolin. Géotechnique 37 (4), 499–503.

Barron, R.A., 1948. Consolidation of fine grained soils by drain wells. Trans. ASCE 113, 718–724.

Bienen, B., Ragni, F., Cassidy, M.J., Stanier, S.A., 2015. Effects of consolidation under a penetrating footing in carbonate silty clay. J. Geotech. Geoenviron. Eng. 141 (9), 04015040.

Craig, W.H., Chua, K., 1990. Extraction forces for offshore foundations under undrained loading. ASCE J. Geotech. Eng. 116 (5), 868–884.

Dean, E.T.R., 2010. Offshore Geotechnical Engineering – Principles and Practice. Thomas Telford, Reston, VA, U.S.A., p. 520.

Gan, C.T., Leung, C.F., Cassidy, M.J., Gaudin, C., Chow, Y.K., 2012. Effect of time on spudcan-footprint interaction in clay. Géotechnique 62 (5), 401–413.

Hodder, M.S., White, D.J., Cassidy, M.J., 2013. An effective stress framework for the variation in penetration resistance due to episodes of remoulding and reconsolidation. Géotechnique 63 (1), 30–43.

Hossain, M.S., Safinus, S., Cassidy, M.J., 2015. Using a thin sand layer to ease spudcan extraction in clay. Can. Geotech. J. 52 (8), 1023–1034.

Houlsby, G.T., Hitchman, R., 1988. Calibration chamber tests of a cone penetrometer in sand. Géotechnique 38 (1), 39–44.

Hu, P., Cassidy, M.J., 2017. Predicting jack-up spudcan installation in sand overlying stiff clay. Ocean Eng. 146, 246–256.

Hu, P., Stanier, S.A., Cassidy, M.J., Wang, D., 2014. Predicting peak resistance of spudcan penetrating sand overlying clay. J. Geotech. Geoenviron. Eng. 140 (2), 04013009.

Hu, P., Stanier, S.A., Wang, D., Cassidy, M.J., 2016. Effect of footing shape on penetration in sand overlying clay. Int. J. Phys. Model. Geotech. 16 (3), 119–133.

International Organization for Standardization (ISO), 2012. Petroleum and natural gas industries – Site-specific assessment of mobile offshore unit-Part 1: Jack-ups. ISO, Geneva, ISO/FDIS 19905-1.

Kohan, O., 2015. Improving spudcan extraction from deep embedment in soft soils. Ph.D. thesis, University of Western Australia, Perth, Australia.

Kohan, O., Gaudin, C., Bienen, B., Cassidy, M.J., 2014a. Spudcan extraction from deep embedment in soft clay. Appl. Ocean Res. 48, 126–136.

Kohan, O., Gaudin, C., Cassidy, M.J., Bienen, B., 2014b. Predicting spudcan extraction resistance in soft clay. Geotechnical Engineering Journal of the South East Asian Geotechnical Society and AGSSEA. Special Edition on Offshore and Coastal Geotechnics 45 (4), 52–61.

Lee, K.K., 2009. Investigation of potential spudcan punch-through failure on sand overlying clay soils. Ph.D. thesis, University of Western Australia, Perth, Australia.

Lee, K.K., Cassidy, M.J., Randolph, M.F., 2013. Bearing capacity on sand overlying clay soils: Experimental and finite element investigation of potential punch-through failure. Géotechnique 63 (15), 1271–1284.

Lehane, B.M., O'Loughlin, C.D., Gaudin, C., Randolph, M.F., 2009. Rate effects on penetrometer resistance in kaolin. Géotechnique 59 (1), 41–52.

Mayne, P.W., Kulhawy, F.H., 1982. K_0-OCR relationships in soil. J. Geotech. Eng. Div., ASCE 108 (GT6), 851–872.

McClelland, B., Young, A.G., Remmes, B.D., 1981. Avoiding jack-up rig foundation failures. Proceedings of the International Symposium on Geotechnical Aspects of Coastal and Offshore Structures, Bangkok.

Muir Wood, D., 1990. Soil Behaviour and Critical State Soil Mechanics. Cambridge University Press, Cambridge.

Purwana, O.A., 2007. Centrifuge Model Study on Spudcan Extraction in Soft Clay. PhD. thesis. National University of Singapore, Singapore.

Purwana, O.A., Leung, C.F., Chow, Y.K., Foo, K.S., 2005. Influence of base suction on extraction of jack-up spudcans. Géotechnique 55 (10), 741–753.

Randolph, M.F., Cassidy, M.J., Gourvenec, S.M., Erbrich, C., 2005. Challenges of offshore geotechnical engineering. Proceedings of the 16th International Conference on Soil Mechanics and Geotechnical Engineering, Osaka, 1, 123–176.

Randolph, M.F., Low, H.E., Zhou, H., 2007. In situ testing for design of pipeline and anchoring systems. In: Proceedings of the 6th International Conference on Offshore Site Investigation and Geotechnics, Society for Underwater Technology, London, pp. 251–262.

Safinus, S., 2016. Estimation of spudcan penetration resistance in stratified soils directly from field penetrometer data and quantification of punch-through risk. Ph.D. thesis, University of Western Australia, Perth, Australia.

Sahdi, F., White, D.J., Gaudin, C., 2017. Experiments using a novel penetrometer to assess the changing strength of clay during remolding and reconsolidation. J. Geotech. Geoenviron. Eng. 143 (4), 1–7.

Stanier, S.A., Blaber, J., Take, W., White, D.J., 2015. Improved image-based deformation measurement for geotechnical applications. Can. Geotech. J. 53 (5), 727–739.

Stanier, S.A., White, D.J., 2013. Improved image-based deformation measurement in the centrifuge environment. Geotech. Test. J. 36 (6), 915–928.

Stewart, D.P., 1992. Lateral loading of pile bridge abutments due to embankment construction. PhD thesis University of Western Australia.

Stewart, D.P., Finnie, I.M.S., 2001. Spudcan-footprint interaction during jack-up workovers. Proceedings of the 11th International Offshore and Polar Engineering Conference, Stavanger, Norway, pp. 61–65.

Teh, K.L., Cassidy, M.J., Leung, C.F., Chow, Y.K., Randolph, M.F., Quah, M., 2008. Revealing the bearing capacity mechanisms of a penetrating spudcan through sand overlying clay. Géotechnique 58 (10), 793–804.

Teh, K.L., Leung, C.F., Chow, Y.K., Cassidy, M.J., 2010. Centrifuge model study of spudcan penetration in sand overlying clay. Géotechnique 60 (11), 825–842.

White, D.J., Take, W., Bolton, M., 2003. Soil deformation measurement using Particle Image Velocimetry (PIV) and photogrammetry. Géotechnique 53 (7), 619–631.

White, D.J., Hodder, M.S., 2010. A simple model for the effect on soil strength of remoulding and reconsolidation. Can. Geotech. J. 47 (7), 821–826.

Wroth, C.P., 1984. The interpretation of in-situ soil tests: Rankine Lecture. Géotechnique 34 (4), 449–489.